VICARIOUS CALIBRATION OF THE DESIS IMAGING SPECTROMETER: STATUS AND PLANS

E. Carmona[1], *K. Alonso*[1], *M. Bachmann*[2], *K. Burch*[3], *D. Cerra*[1], *R. de los Reyes*[1], *U. Heiden*[1]
U. Knodt[4], *D. Krutz*[5], *D. Marshall*[1], *R. Müller*[1], *P. Reinartz*[1]

[1]Remote Sensing Technology Institute, DLR, Oberpfaffenhofen, 82234 Wessling, Germany
[2]German Remote Sensing Data Center, DLR, Oberpfaffenhofen, 82234 Wessling, Germany
[3]Innovative Imaging and Research, Corp. (I2R), Stennis Space Center, MS 39529, US
[4]Strategic services, DLR, Linder Höhe, 51147 Köln, Germany
[5]Institute of Optical Sensor Systems, DLR, Rutherfordstrasse 2, 12489 Berlin, Germany

ABSTRACT

The DLR Earth Sensing Spectrometer (DESIS) on board the International Space Station (ISS) has been providing high quality hyperspectral data to the scientific community and commercial users since the start of operations in September 2018. After almost 4 years in orbit, the DESIS instrument continues to operate correctly and to deliver hyperspectral data products for a wide variety of applications. In order to support this successful activity, the calibration team regularly analyzes the instrument data and provides updates using vicarious calibration. We present here the latest results from the DESIS vicarious calibration and our plans for future improvements.

***Index Terms*—** Remote Sensing, Hyperspectral, Spaceborne, Vicarious Calibration

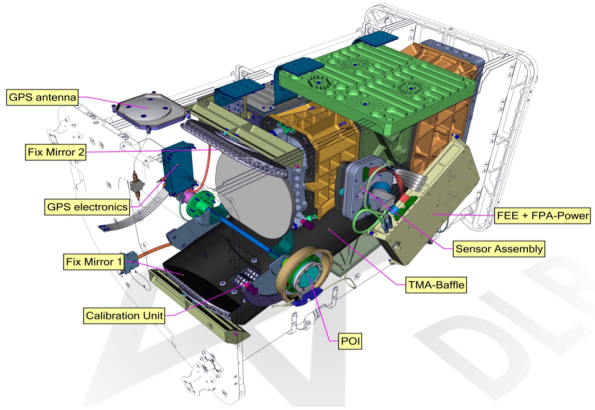

Fig. 1. The DESIS Instrument and its main components.

1. INTRODUCTION

The DESIS instrument was built by the German Aerospace Agency (DLR) who also provides the processing software that produces the DESIS data products. It is installed on board the ISS in one of the 4 slots of the MUSES platform [1]. Teledyne Brown Engineering built and operates this platform as well as it operates the DESIS instrument. DESIS is a push-broom imaging spectrometer observing in the VNIR range ($400 - 1000$ nm) that offers a spectral sampling distance of 2.55 nm. A full description of the instrument and its design can be found in [2]. Figure 1 shows an schematic view of the DESIS instrument and some of its components.

The DESIS image products consist of 235 spectral bands $\times$ 1024 spatial, across-track pixels that are divided every 1024 along-track pixels into so-called *tiles*. Users can order DESIS products with three different processing levels (L1B, L1C, L2A) and different processing options. A complete description of the DESIS data products and DESIS performance can be found in [3]. DESIS products are used in various applications by a growing community of DESIS users, who held an initial user workshop in September 2021. For more details on the access to the DESIS data products and the applications using them see [4].

DESIS calibration is based on the use of vicarious calibration with support from the on-board LED calibration measurements. The instrument was calibrated on-ground [5] and validated during the commissioning phase [3] with an early version of the vicarious calibration. Since then, the vicarious calibration process has been optimized and newer calibration tables are produced regularly, specially to update the radiometric calibration of the instrument. This was the case also for other spaceborne imaging spectrometers like HICO [6], which shows the validity of this approach in the context of hyperspectral missions.

The on-board calibration unit is mainly used to perform small updates on the spectral calibration. Figure 2 shows the relative variation of the pixel central wavelengths obtained from the on-board spectral calibration analysis. The data show that after a first continuous variation at a rate of 0.2 nm

per year, the central wavelength values are stable. Until now the only update required on the spectral calibration has been a global shift of 0.1 nm.

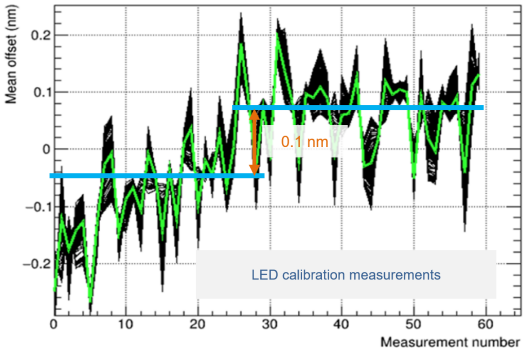

Fig. 2. Relative spectral stability of the DESIS instrument from several on-board calibration measurements performed between January 2019 and October 2020.

2. VICARIOUS CALIBRATION OF THE DESIS INSTRUMENT

The variation of the instrument's response over time requires the update of the calibration coefficients on a regular basis. The main updates are performed on the radiometric calibration coefficients using our vicarious calibration method [7].

As input we use good quality DESIS scenes acquired over different areas. Two types of input scenes are used in our vicarious calibration:

- **Uniform scenes**, typically desert areas that offer good uniformity within an image *tile*. Examples of these areas are the CEOS PICS sites, although in our case temporal stability is not required for the scenes. These data are averaged on the along-track direction to obtain a mean focal plane response for each scene that is later used in a sequence of processing steps (for more details see [7]) to achieve the equalization of the sensor response.

- **RadCalNet [8] scenes** over the sites of Gobabeb, Railroad Valley and La Crau that are used to adjust the absolute radiometric calibration within a given calibration period.

RadCalNet (RCN) observations are regularly scheduled over the pre-selected RCN sites to be used in our vicarious calibration. In the case of the uniform scenes, no special targets are scheduled and we simply select suitable images from the DESIS data archive.

The duration of a period is chosen by taking into account the sensor performance changes and the availability of data to perform a new calibration. A total of 3 periods have been defined up to now. A fourth period starting on the second half of 2021 is in preparation (see section 4). Given the availability of suitable scenes, Period #2 was defined shorter in order to study the advantages of reducing the duration of the periods. In this case no significant difference in performance was observed with respect to Periods #1 or #3, except for the wavelength range under 450 nm where the sensor shows the highest variability. On the other hand, shorter periods will face the problem of data availability and will increase the effort to maintain the vicarious calibration. An overview of the number of scenes of each type used in the vicarious calibration of the different periods is shown in figure 3.

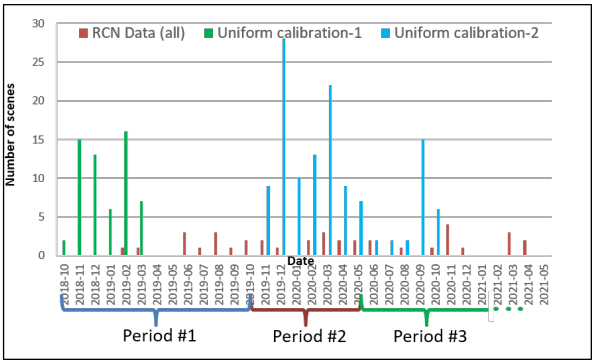

Fig. 3. Calibration periods defined in the DESIS and the different scenes used.

Up to now only period #2 includes a global spectral shift (see figure 2) in addition to the radiometric update. The effect of this spectral shift on the radiometric coefficients is rather small compared with their typical variation over time in the periods with no spectral shift.

3. LATEST RESULTS

For each DESIS pixel (i, j) in the focal plane, the signal value is converted to radiance with the calibration coefficients ($C_{i,j}$) obtained from the relative pixel calibration steps in the vicarious calibration and the original laboratory coefficients. A simple expression provides the radiance values as $L_{i,j} = C_{i,j} \cdot (DN_{i,j} - DN^0_{i,j})$ where $DN_{i,j}$ is the measured sensor value, $DN^0_{i,j}$ is the dark current value and $C_{i,j}$ is the updated calibration factor. We use the ratio of RCN to DESIS TOA reflectance in order to compute a per-band coefficient (f_i^{corr}) that corrects the bias between DESIS and RCN. This is convenient given that TOA reflectance is directly provided by RCN. This factor is applied on the radiance values after smile correction ($\tilde{L}_{i,j}$) where an interpolation of the values on the spectral direction ($\tilde{L}_{i,j} = f_{int}(L_{i-2,j}, L_{i-1,j}, ..., L_{i+2,j})$ is performed (see [3]). The final radiance values are obtained as $\tilde{L}^{final}_{i,j} = \tilde{L}_{i,j} \cdot f_i^{corr}$.

For the absolute calibration task we select only scenes

with Sun zenith angle below 45 degrees and good atmospheric conditions. From a total of 30 RCN scenes in the three calibration periods currently defined, only 19 fulfill this condition. An example of the calculation of the bias correction can be seen in figure 4 where the TOA reflectance ratio computed for each band is fitted using a polynomial. The fit is then used to compute a per-band correction factor that will be used to update the individual pixel calibration coefficients. The regions with strong atmospheric absorption are excluded from the fit (in the figure the black color points).

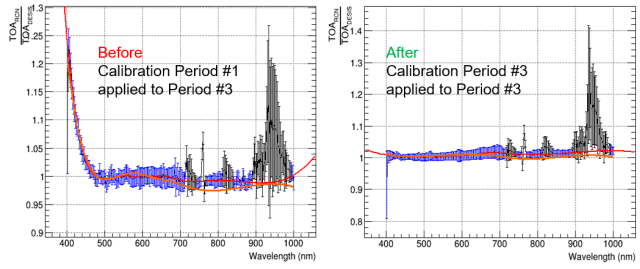

Fig. 4. Example of the absolute calibration adjustment on the DESIS data. Left: Ratio between DESIS TOA reflectance and RCN TOA reflectance on Period #3 using the original calibration coefficients from Period #1. Right: Ratio between DESIS TOA reflectance and RCN TOA reflectance on Period #3 once the calibration coefficients have been updated. The red lines show examples of the polynomial fit to the data.

Two main observations can be made from figure 4. First, bands above 450 nm show little variation over a period of more than a year between Period #3 and Period #1 (difference typically $\leq$ 2%). Second, bands below 450 nm show an important degradation over the same amount of time. It is maximum at 400 nm, with a rate of change around 20%/year, and it reduces continuously until disappearing in the range $460 - 480$ nm.

Figure 5 shows the ratio of TOA reflectances for the 19 measurements used for the radiometric update, after calibration is updated for each period. In order to reduce the systematic errors, two estimates of the TOA reflectance ratio are averaged in our calculations. One is computed using directly the RCN TOA values of reflectance and corresponds to a spectral sampling distance of 10 nm (figure 5 left). The other one is computed by ourselves from the RCN BOA spectra after performing an inversion of the atmospheric correction [9] used in DESIS L2A and corresponds to the spectral sampling distance of the DESIS instrument (figure 5 right).

Since the absolute bias of the calibration scenes is adjusted to match the RCN data, it is not possible to use this metric for our second purpose, the estimation of the calibration performance. What we use instead are the RMS values obtained from the comparison with RCN. The value obtained from the 19 calibration scenes is between 3% and 4%, outside

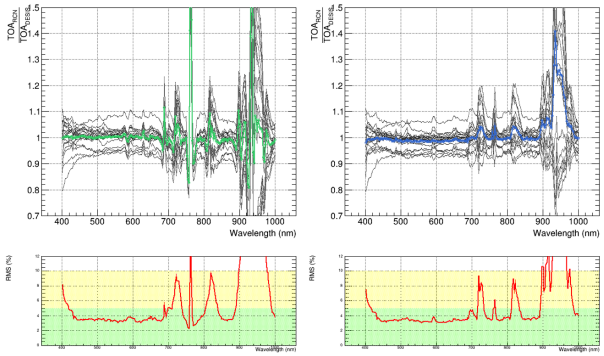

Fig. 5. Top: ratio of TOA reflectances between RCN and DESIS for the TOA reflectance provided by RCN (left) and computed by us (right). The black lines show the 19 individual scenes used for calibration purposes while the color line corresponds to their mean value. Bottom: RMS values computed from the corresponding top plots.

the strong atmospheric absorption regions and above 450 nm. In addition, we look at the performance of the calibration for the full dataset of RCN scenes (30 scenes) that include those with Sun zenith angle above 45 degrees as well as those with not optimal atmospheric conditions. The results after analyzing the full dataset can be seen in figure 6. In this case we notice that while the bias is not significantly affected, the RMS is now increased to an average value around 4%. These results agree well with those from independent investigations using DESIS and RCN data as conducted in [10] and [11].

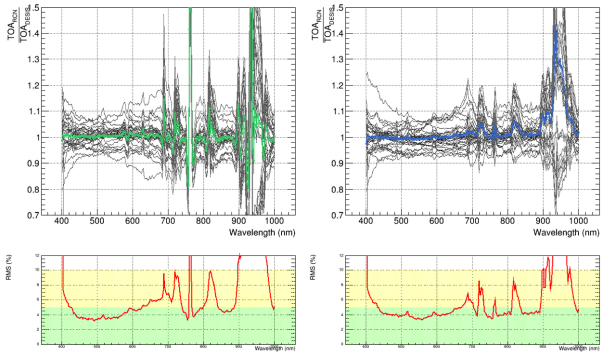

Fig. 6. Top: ratio of TOA reflectances between RCN and DESIS for the TOA reflectance provided by RCN (left) and computed by us (right). The black lines show the total of 30 available scenes and the color line corresponds to their mean value. Bottom: Root Mean Square values computed from the corresponding top plots.

In both datasets (calibration and full one) we observe that the RMS performance degrades quickly as the wavelength reduces below 450 nm. Our current approach using calibration

periods can adjust the calibration coefficients to correct the mean bias of each period but can't reduce the dispersion below 450 nm due to the rapid change of performance. The reason for this degradation is not known yet, but we suspect it could be caused by a degradation on the coating of the mirrors, more specifically of the mirror in the Pointing Unit. The next section presents our plans to address this limitation.

4. FUTURE PLANS

Our calibration strategy was designed to support small instrument changes over time or sudden larger changes at well identified intervals. However, the rapid change in performance in region below 450 nm is not well handled by this approach and requires a different strategy. The sparse RCN acquisitions do not allow us to build a detailed model based only on them. Given this, we plan to use the on-board LED calibration data to build a 2D model of the sensor response changes over time for the different spectral bands and across-track pixels. Our investigations indicate that this performance degradation is constant in time although the magnitude varies for the different across-track elements in addition to the different magnitude at different wavelengths. The difference between a model with linearly changing calibration coefficients and our current approach is illustrated in figure 7. From this illustration one can see that the existing approach introduces larger calibration errors at the edges of the calibration periods and it creates artificial calibration jumps when changing from one period to the next. We plan to introduce this change together with a new calibration period once the analysis of all the data is concluded.

Although there are certain difficulties in the development of such a calibration model and its application to the data from all periods, we expect that this would improve the calibration performance below 450 nm. This would also improve the calibration performance for new acquisitions, provided that the validity of the sensor changes model continues to apply.

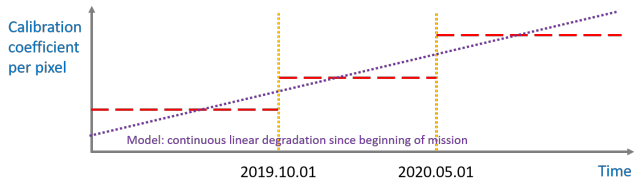

Fig. 7. Illustration of the difference between current calibration approach and linear calibration update model.

5. REFERENCES

[1] R. Perkins and P. Galloway et al., "Teledyne's MUSES mission on the ISS: Enabling flexible and reconfigurable earth observation from space," in *2017 IEEE International Geoscience and Remote Sensing Symposium (IGARSS)*, 2017, pp. 1177–1180.

[2] D. Krutz, R. Müller, and U. Knodt et al., "The Instrument Design of the DLR Earth Sensing Imaging Spectrometer (DESIS)," *Sensors*, vol. 19, pp. 1622, 2019.

[3] K. Alonso, M. Bachmann, and K. Burch et al., "Data Products, Quality and Validation of the DLR Earth Sensing Imaging Spectrometer (DESIS)," *Sensors*, vol. 19, no. 20, pp. 4471, 2019.

[4] D. Cerra, D. Marshall, and U. Heiden et al., "The spaceborne imaging spectrometer desis: Data access, outreach activities, and scientific applications," in *2022 IEEE International Geoscience and Remote Sensing Symposium IGARSS*, 2022.

[5] I. Sebastian, D. Krutz, and A. Eckardt et al., "On-ground calibration of DESIS: DLR's Earth Sensing Imaging Spectrometer for the International Space Station (ISS)," in *Optical Sensing and Detection V*, Francis Berghmans and Anna G. Mignani, Eds. International Society for Optics and Photonics, 2018, vol. 10680, pp. 1 – 12, SPIE.

[6] Bo-Cai Gao, Rong-Rong Li, and Robert L. Lucke et al., "Vicarious calibrations of HICO data acquired from the international space station," *Appl. Opt.*, vol. 51, no. 14, pp. 2559–2567, May 2012.

[7] E. Carmona, K. Alonso, and M. Bachmann et al., "Vicarious calibration of the desis imaging spectrometer," in *2021 IEEE International Geoscience and Remote Sensing Symposium IGARSS*, 2021, pp. 1611–1614.

[8] M. Bouvet, K. Thome, and B. Berthelot et al., "RadCalNet: A Radiometric Calibration Network for Earth Observing Imagers Operating in the Visible to Shortwave Infrared Spectral Range," *Remote Sensing*, vol. 11, no. 20, 2019.

[9] R. de los Reyes, M. Langheinrich, and P. Schwind et al., "PACO: Python-Based Atmospheric Correction," *Sensors*, vol. 20, no. 5, 2020.

[10] M. Shrestha, D. Helder, and J. Christopherson, "Dlr earth sensing imaging spectrometer (desis) level 1 product evaluation using radcalnet measurements," *Remote Sensing*, vol. 13, no. 12, 2021.

[11] M. Shrestha, A. Sampath, and S.N. Ramaseri Chandra et al., "System characterization report on the german aerospace center (dlr) earth sensing imaging spectrometer (desis)," *System characterization of Earth observation sensors: U.S. Geological Survey Open-File Report 2021-1030, 9 p.*